Biogeosciences Discuss., 8, 5617–5652, 2011
www.biogeosciences-discuss.net/8/5617/2011/
doi:10.5194/bgd-8-5617-2011

Biogeosciences Discussions

What controls biological productivity in coastal upwelling systems? Insights from a comparative modeling study

Z. Lachkar and N. Gruber

Environmental Physics, Institute of Biogeochemistry and Pollutant Dynamics, ETH Zurich, Universitätstrasse 16, 8092 Zurich, Switzerland

Received: 29 May 2011 – Accepted: 30 May 2011 – Published: 14 June 2011

Correspondence to: Z. Lachkar (zouhair.lachkar@env.ethz.ch)

Published by Copernicus Publications on behalf of the European Geosciences Union.

Abstract

The magnitude of the biological productivity in Eastern Boundary Upwelling Systems (EBUS) is traditionally viewed as directly reflecting the upwelling intensity. Yet, different EBUS show different sensitivities of productivity to upwelling-favorable winds (Carr and Kearns, 2003). Here, using a comparative modeling study of the California Current System (California CS) and Canary Current System (Canary CS), we show how physical and environmental factors, such as light, temperature and cross-shore circulation modulate the response of biological productivity to upwelling strength. To this end, we made a series of eddy-resolving simulations of the California CS and Canary CS using the Regional Ocean Modeling System (ROMS), coupled to a nitrogen based Nutrient-Phytoplankton-Zooplankton-Detritus (NPZD) ecosystem model. We find the nutrient content of the euphotic zone to be 20 % smaller in the Canary CS relative to the California CS. Yet, the biological productivity is 50 % smaller in the latter. This is due to: (1) a faster nutrient-replete growth in the Canary CS relative to the California CS, related to a more favorable light and temperature conditions in the Canary CS, and (2) the longer nearshore water residence times in the Canary CS which lead to larger buildup of biomass in the upwelling zone, thereby enhancing the productivity. The longer residence times in the Canary CS appear to be associated with the wider continental shelves and the lower eddy activity characterizing this upwelling system. This results in a weaker offshore export of nutrients and organic matter, thereby increasing local nutrient recycling and enhancing the coupling between new and export production in the Northwest African system. Our results suggest that climate change induced perturbations such as upwelling favorable wind intensification might lead to contrasting biological responses in the California CS and the Canary CS, with major implications for the biogeochemical cycles and fisheries in these two ecosystems.

BGD

8, 5617–5652, 2011

1 Introduction

Eastern boundary upwelling systems (EBUS) are among the most productive marine ecosystems in the world and are well known for supporting some of the world's major fisheries (Pauly and Christensen, 1995; Bakun, 1990; Carr, 2001; Carr and Kearns, 2003; FAO, 2009). Although they represent less than 1 % of the world ocean by area, EBUS account for around 11 % of global new production (Chavez and Toggweiler, 1995) and up to 20 % of the global fish catch (Pauly and Christensen, 1995). This high productivity supports large downward export of organic carbon (Muller-Karger et al., 2005), in addition to a significant fraction which is exported laterally into the open ocean (Aristegui et al., 2004). Thus, determining what controls productivity within EBUS is not only essential to understand the functioning of these ecosystems, but is also relevant to the assessment of the global marine carbon cycle.

The high productivity in EBUS is driven, to the first order, by the upwelling of nutrient-rich water associated with the equatorward winds along the eastern boundaries of the Atlantic and Pacific (Allen, 1973; Brink, 1983a). Yet, individual upwelling systems show substantial differences in net primary production (NPP) for reasons that remain neither well understood nor well quantified (Carr, 2001; Thomas et al., 2001; Carr and Kearns, 2003; Lachkar et al., 2011). Here, we examine the productivity drivers in EBUS with a particular focus on the mechanisms that control the sensitivity of biological production to upwelling intensity.

To this end, we contrasted two of the four major EBUS, namely the California Current System (California CS) and the Canary Current System (Canary CS). Our goal is to identify the major limitations of biological productivity in these systems and to improve our understanding of how different environmental and physical conditions can alter the sensitivity of productivity to the wind forcing in EBUS. The comparison of the two systems provides a framework for developing a more comprehensive view of the factors that influence the sensitivity of biological production to wind forcing and for a better understanding of the underlying dynamics of EBUS ecosystems in general (Lachkar

BGD
8, 5617–5652, 2011

et al., 2011). This can also be useful for predicting response of EBUS under potential wind changes induced by climate change (Bakun, 1990; Shannon et al., 1992; Mendelssohn, 2002; McGregor et al., 2007).

Over the last decade, several comparative studies of EBUS have been conducted using satellite observations to identify commonalities and differences in the production regimes characterizing these systems (Thomas et al., 2001; Carr, 2001; Carr and Kearns, 2003; Demarcq, 2009; Lachkar et al., 2011). For instance, Demarcq (2009) showed that recent observed changes in surface chlorophyll and productivity in EBUS are only moderately correlated with changes in wind, suggesting a contrasting sensitivity of the productivity to the upwelling changes in the different EBUS. Using a Self-Organizing Map (SOM) analysis of recent satellite data, Lachkar et al. (2011) found that the sensitivity of biological production to upwelling-favorable wind is fundamentally different between the Atlantic and the Pacific EBUS, and proposed parameters such as the width of continental shelf and the level of eddy activity as factors potentially explaining these contrasts. Adopting a modeling approach is needed to test these hypotheses and gain a mechanistic understanding of the underlying dynamics controlling production in EBUS. Yet, because of the lack of portable regional models tested and validated over distinct upwelling systems, to our knowledge no comparative modeling study of production regimes in EBUS has been proposed. Here we show how by using the same model with identical settings for two different EBUS, one can gain insight into the sensitivity of biological production to the local physical and environmental conditions. Finally, by modeling the California CS and the Canary CS at an eddy-resolving resolution, we aim at properly capturing the role of the mesoscale variability. Previous studies have, indeed, shown that eddies are particularly important for the dynamics of EBUS (Rossi et al., 2008; Marchesiello and Estrade, 2009; Gruber et al., 2011).

BGD
8, 5617–5652, 2011

2 Methods

2.1 Model details

2.1.1 The circulation model

Our circulation model is based on UCLA version of the Regional Ocean Modeling System (ROMS) (Shchepetkin and McWilliams, 2005). ROMS solves the primitive equations with a free sea surface, horizontal curvilinear coordinates, and a generalized terrain-following vertical coordinate (Marchesiello et al., 2003; Shchepetkin and McWilliams, 2005). The open-boundary conditions are a combination of outward radiation and flow-adaptive nudging toward prescribed external conditions (Marchesiello et al., 2001). Advection is represented using a third order and upstream biased operator, designed to reduce dispersive errors and the excessive dissipation rates needed to maintain smoothness (Shchepetkin and McWilliams, 1998). Vertical diffusivity in the interior and planetary boundary layers is given by the nonlocal K-Profile Parameterization (KPP) scheme (Large et al., 1994).

The bathymetry is calculated using the $2'$ bathymetry file ETOPO2 from the National Geophysical Data Center (Smith and Sandwell, 1997). Depths shallower than 50 m are reset to 50 m. After interpolation and truncation, the topography is smoothed using a selective Shapiro filter for excessive topographic slope parameter values (Beckmann and Haidvogel, 1993) to avoid large pressure gradient errors.

2.1.2 The Ecosystem model

The ecological-biogeochemical model is a nitrogen based NPZD model described in detail by Gruber et al. (2006). It consists of a system of seven coupled partial differential equations that govern the time and space distribution of the following non-conservative scalars: nitrate (NO_3^-) subsequently denoted as N_n to reflect "new" nitrogen, ammonium (NH_4^+), denoted as N_r to reflect regenerated nitrogen, phytoplankton

BGD
8, 5617–5652, 2011

(P), zooplankton (Z), small (D_S) and large (D_L) detritus, and a dynamic phytoplankton chlorophyll-to-carbon ratio (θ).

The model has two pools of detritus, a large one that sinks fast, and a small one that sinks slowly. The small detrital pool coagulates with phytoplankton, thereby forming large, fast sinking detritus. Sinking is modeled explicitly, thereby permitting all state variables to be advected laterally even in the aphotic zone.

The biological source minus sink flux for phytoplankton, $J(P)$, is given by:

$$J(P) = \mu_P(T,I,N_n,N_r)\cdot P - \Phi^{graz}(P,Z)\cdot P - \Phi^{mort}\cdot P - \Phi^{coag}(P,D_S)\cdot P \quad (1)$$

The first term on the right-hand side of Eq. (1) is primary production with $\mu_P(T,I,N_n,N_r)$ being the growth rate of phytoplankton. The other three terms represent, grazing, mortality and coagulation, respectively. Phytoplankton growth is limited in our model by the amount of photosynthetically available radiation (PAR), I, the concentrations of nitrate, N_n, and ammonium, N_r and temperature, T in the following manner:

$$\mu_P(T,I,N_n,N_r) = \mu_P^{max}(T,I)\cdot\gamma(N_n,N_r) \quad (2)$$

where $\mu_P^{max}(T,I)$ is the temperature-dependent, light-limited growth rate under nutrient replete conditions and $\gamma(N_n,N_r)$ is a non-dimensional nutrient limitation factor. The temperature-dependent, light-limited growth rate is given by:

$$\mu_P^{max}(T,I) = \frac{\mu_P^T(T)\cdot\alpha_P\cdot I\cdot\theta}{\sqrt{(\mu_P^T(T))^2+(\alpha_P\cdot I\cdot\theta)^2}} \quad (3)$$

where α_P is the initial slope in the growth versus light relationship and θ the dynamic phytoplankton chlorophyll-to-carbon ratio. The temperature-dependent growth rate $\mu_P^T(T)$ is parameterized using the relationship of Eppley (1972):

$$\mu_P^T(T) = \ln 2\cdot 0.851\cdot(1.066)^T \quad (4)$$

The nutrient limitation factor $\gamma(N_n,N_r)\leq 1$, is parameterized using a Michaelis–Menten equation, taking into account that ammonium is taken up preferentially over nitrate, and

BGD
8, 5617–5652, 2011

that its presence inhibits the uptake of nitrate by phytoplankton (Wroblewski, 1977). We use an additive function weighted toward ammonium:

$$\gamma(N_n, N_r) = \gamma(N_n) + \gamma(N_r) = \frac{N_n}{K_{N_n} + N_n} \frac{K_{N_r}}{K_{N_r} + N_r} + \frac{N_r}{K_{N_r} + N_r} \quad (5)$$

where K_{N_n} and K_{N_r} are the half-saturation constants for phytoplankton uptake of nitrate and ammonium, respectively. Further details of the ecosystem model equations and parameters are given in Gruber et al. (2006).

2.2 Model setup

For the purpose of our comparative study, we developed two ROMS configurations for the California CS and the Canary CS. In the California CS the domain extends in latitude from the middle of Baja California (28° N) to the Canadian border (48° N). This is about 2000 km alongshore and 1000 km offshore, and it encompasses the California CS and its most energetic eddy region. This is the same setup used in Gruber et al. (2006). In the Canary CS the domain extends in latitude from 10° N (latitude of the North Equatorial Current) to 43° N (North-West Iberia). This is about 3200 km alongshore and 1500 to 2500 km offshore, and it encompasses the entire Canary CS and its different subsystems (Aristegui et al., 2009).

For both configurations the horizontal grid spacing is 5 km, allowing an explicit resolution of most of the mesoscale eddy spectrum (Chassignet and Verron, 2006). The vertical grid has 32 levels with surface refinement. The stretching parameters for the vertical grid allow for a reasonable representation of the surface boundary layer and the euphotic zone everywhere in the domain. On average, about eight levels are within the euphotic zone, defined here as the 1 % light level.

Initial and boundary conditions for the temperature, salinity and nitrate fields were taken from the World Ocean Atlas 2005. The model was started from rest, then spun up for 10 years with a climatological monthly forcing. Wind stress is taken from

BGD
8, 5617–5652, 2011

the QuikSCAT-based Scatterometer Climatology of Ocean Winds (SCOW) (Risien and Chelton, 2008). The surface heat and freshwater fluxes were derived from the Comprehensive Ocean-Atmosphere Data Set (COADS) (da Silva et al., 1994) and applied with a surface temperature and salinity restoring following the formulation of Barnier et al. (1995). In order to remove the model internal chaotic interannual variability, we generally show and discuss 5-year averages from model years 6 to 10.

We quantitatively compare the simulations from the two systems as follows: data are averaged for both systems, extending from the coastline to 300 km offshore and over 1° bins in meridional direction from 30° N to 46° N for the California CS, and from 12° N to 28° N for the Canary CS. These boundaries were chosen to include the most productive regions of these upwelling systems.

2.3 Model evaluation

Our model is similar to the one described and evaluated earlier in Gruber et al. (2006) with two major differences. First, this model is run at 5 km resolution throughout the domain, while the previous one had a 15 km resolution over the entire domain, and employed a 5 km child grid for the central California CS. Second, the model is based on a newer numerical core optimized for computations on distributed systems (A. Shchepetkin, personal communication, 2008). Additional modifications include an improved implementation of the KPP scheme, a stiffer scheme for the vertical sigma coordinate system and improved numerics for tracer transport. These changes are substantial enough to require a re-evaluation of the model's performance on the basis of primarily satellite chlorophyll and sea-surface temperature (SST), augmented with a monthly climatology of mixed layer depth based on the Argo float observations.

Simulated annual mean surface chlorophyll-*a* concentrations compare generally well to SeaWiFS in both the California CS and the Canary CS, although there is an important underestimation of nearshore concentrations (Fig. 1). The model-data discrepancies in the coastal zone may partially be due to a systematic bias in the SeaWiFS data towards higher concentrations in the coastal waters. Indeed, ocean color remote

BGD
8, 5617–5652, 2011

sensing tends to generally overestimate chlorophyll in continental shelf and coastal regions because of increased concentrations of colored optical constituents in the water that vary independently of phytoplankton chlorophyll pigment and absorbing aerosols that tend to be concentrated near the coast (Schollaert et al., 2003; Hyde et al., 2007). This is also consistent with previous results from Gruber et al. (2006) who found similar discrepancies by comparing SeaWiFS chlorophyll with those measured in situ by the CalCOFI program in this region.

The simulated annual mean SST represents well the observed pattern in both the California CS and Canary CS (Fig. 2). In particular, the model successfully captures the offshore extent of the cold upwelling region in both systems. However, as found by Gruber et al. (2006), absolute values of modeled SST exhibit a cold bias of about 1 °C relative to AVHRR satellite data in most of the California CS as well as in the northern Canary CS. Some of the differences between the model and the data likely reflect true changes over time, since our model was forced with heat fluxes from the COADS climatology, which was derived from observations collected between 1950 to 1989, whereas the AVHRR climatology was put together on the basis of the years 1997–2005 only. Therefore, the long-term surface ocean warming observed over the last couple of decades will likely lead to higher SST in AVHRR data in comparison with COADS.

A more quantitative evaluation of the model simulations is depicted in the Taylor (2001) diagrams shown in Fig. 3. A Taylor diagram is an $r - \theta$ polar plot that provides a quick quantitative synthesis of three statistics. First, the modeled field's standard deviation relative to the standard deviation of data is represented by the radius r (distance on the plot between the model and the origin point). Second, the angle θ between the model point and the x-axis indicates the correlation coefficient between the model and the data reference. Finally, the distance from the reference point to a given modeled field represents that field's central pattern root mean square (RMS), also known as the pattern error. If a model were perfect, it would lie along the x-axis, right on top of the (observation) reference point.

BGD
8, 5617–5652, 2011

For both the California CS and the Canary CS, we find relatively high correlations between simulated and satellite-based annual mean surface chlorophyll ranging between 0.68 for the nearshore area of the California CS up to around 0.9 for the Canary CS when estimated over the entire domain (Fig. 3a). The standard deviations of simulated chlorophyll patterns are, however, 30 % to 50 % lower than in SeaWiFS. This is essentially due to the model underestimating SeaWiFS's high values in the immediate nearshore as we mentioned before. The simulated surface temperatures show high agreement with SST observations from AVHRR (Fig. 3a). In particular, the correlations between modeled and observed patterns are particularly high ranging between 0.95 and 0.99. Finally, the correlation between the simulated mixed layer depth and the Argo-based climatology of de Boyer Montégut et al. (2004) is around 0.7 in the California CS and 0.85 in the Canary CS (Fig. 3a). As nearshore MLD observations are associated with relatively large uncertainties (few Argo floats in the coastal areas), only the patterns related to the entire domain are represented in the Taylor diagrams. In both systems, the modeled mixed layer depths have substantially larger standard deviations relative to observations. This is likely due to the much coarser resolution of the data (2°) in comparison to our model's fine resolution of 5 km.

The model simulates the seasonal cycle of chlorophyll less successfully than the annual mean pattern (Fig. 3b). In both the California CS and the Canary CS, the correlations of the seasonal anomalies, i.e. of the monthly means minus the annual means, range between 0.3 and 0.45. This distinct difference between the annual mean and the seasonal component is not reflected in the SST, which shows generally a very good agreement with observations with a correlation around 0.95 and a model variance very close to the observed one. For the mixed layer depth, the correlations of the seasonal anomalies with observations are 0.75 and 0.82 for the Canary CS and the California CS, respectively. In both systems, the model variance is substantially larger than in observations. Again, this is likely due to the coarse resolution of the mixed layer climatology.

BGD
8, 5617–5652, 2011

Overall, the model exhibits reasonable skills in both upwelling systems and shows a better agreement with observations than the previous version used in Gruber et al. (2006). Next, we compare the biological productivity between the two systems, and we explore the mechanisms responsible for their contrasts.

3 Results

The simulated NPP is largest south of Cape Bojador (around 26° N) in the Canary CS and between 34° N and 38° N in the California CS (Fig. 4). The Canary CS generally shows higher productivity in comparison to the California CS. According to Eq. (1), biological productivity can be expressed as the product of the nutrient limitation term $\gamma(N_n, N_r)$, the nutrient-unlimited growth rate $\mu_P^{max}(T, I)$ and the biomass P. Therefore, we need to examine each of these three components in order to understand the contrasting productivities between the two systems.

3.1 Biological productivity and nutrient resources in the California and Canary systems

As the high biological productivity in EBUS is driven to the first order by the upwelling of nutrient-rich water to the surface, these differences may simply result from contrasting upwelling intensities between the two systems leading to different nutrient concentrations in the euphotic zone. To test this hypothesis, we examine here the relationship between NPP and the nutrient content in the euphotic zone in the two upwelling systems (Fig. 5a). To this end, we computed for each system the total inorganic nitrogen TIN (i.e., nitrate and ammonium) integrated vertically over the euphotic zone.

While the productivity is 54 % larger in the Canary CS relative to the California CS, the TIN concentrations are on average 18 % larger in the latter (Table 1). Furthermore, in both systems and particularly in the California CS, the relationship between the productivity and the TIN exhibits a strong non-linearity, with a relative saturation

BGD
8, 5617–5652, 2011

of productivity at high nutrient concentrations. A part of this non-linearity is due to the Michaelis-Menten nutrient limitation formulation which is strongly non-linear with respect to nutrient concentrations. Thus, to better describe the relationship between productivity and the "useful" nutrient resources, we show in Fig. 5b the NPP as a function of the nutrient limitation factor $\gamma(N_n, N_r)$. In both systems, substantially larger linear correlations exist between NPP and $\gamma(N_n, N_r)$ than that between NPP and TIN. The slopes of a linear regression of NPP on the nutrient limitation factor $\gamma(N_n, N_r)$ vary from $19.88(\pm 6.63)\,\mathrm{mol\,C\,m^{-2}\,yr^{-1}}$ for the California CS to $49.72(\pm 7.64)\,\mathrm{mol\,C\,m^{-2}\,yr^{-1}}$ for the Canary CS. While strongly correlated with productivity in both systems, the nutrient concentrations and hence the upwelling intensity clearly do not explain the contrasting levels of NPP between the two upwelling systems.

In order to understand why nutrients are more efficiently used in the Canary CS than in the California CS, we need to examine the the other drivers of productivity, besides the availability of nutrients. Next, we investigate the phytoplankton growth under nutrient-replete conditions and how it varies between the two systems.

3.2 The nutrient-replete growth rate in the California CS and Canary CS

The comparison of the two systems reveals that the nutrient-replete growth rate $\mu_P^{max}(T,I)$ is, on average, 40 % faster in the Canary CS than in the California CS (Table 1 and Fig. 6). As described by Eq. (3), $\mu_P^{max}(T,I)$ is a function of light, temperature and the dynamic chlorophyll-to-carbon ratio θ. In order to better understand the contribution of each of these three factors to the overall difference in $\mu_P^{max}(T,I)$ between the two systems, we consider normalized $\mu_P^{max}(T,I)$ distributions with respect to light, the chlorophyll-to-carbon ratio, and temperature, respectively (Fig. 6).

When normalized to a constant PAR of $20\,\mathrm{W\,m^{-2}}$ that corresponds to the average light conditions in the central California CS, the average nutrient-replete growth rate becomes smaller in the Canary CS than in the California CS (Table 1). That is, if both systems were exposed to identical light conditions, the nutrient-replete growth $\mu_P^{max}(T,I)$ in the California CS would have slightly exceeded that from the Canary

BGD
8, 5617–5652, 2011

CS. This indicates a dominant role of the light resources in the contrasting nutrient-replete growth rates between the two systems. The large magnitude of light control on $\mu_P^{max}(T,I)$ is, however, attenuated by the chlorophyll-to-carbon ratio variations allowed in our model, which mimic photoacclimation in phytoplankton (Falkowski and Raven, 1997). Fixing θ for example at 25 mg C (mg chl-a)$^{-1}$, which corresponds to the average conditions in the central California CS, enhances indeed the difference in $\mu_P^{max}(T,I)$ between the two systems by more than 50 % (Table 1). Finally, when normalized to a constant temperature of 20 °C, the difference in $\mu_P^{max}(T,I)$ between the two systems gets reduced by 35 %, which indicates a smaller yet important role played by the temperature differences in the contrasting nutrient-replete growth rates between the two upwelling systems (Table 1).

The 40 % faster μ_P^{max} in the Canary CS results in the overall growth rate μ_P being 12 % larger in this system, despite a higher nutrient limitation (Table 1). Does this difference explain alone the more than 50 % larger productivity in the Canary CS relative to the California CS? To answer this question, we next consider the effect of the third component in Eq. (1), i.e., the phytoplankton biomass, on the productivity in the two upwelling systems.

3.3 Productivity and the phytoplankton biomass in the California CS and Canary CS

The correlation between the biological production and the growth rate is very strong in both systems with R^2 of 0.93 and 0.97 in the Canary and the California systems, respectively. Yet, comparable growth rates in the Canary CS and the California CS lead to substantially different productivities (Fig. 7). The slopes of a linear regression of NPP on the growth rate vary from 99.98(±9.63) mol C m^{-2} for the California CS to up to 168.08(±27.93) mol C m^{-2} for the Canary CS. This difference indicates a significantly larger average biomass in the Canary CS relative to the California CS even at comparable growth rates. Therefore, in addition to the slightly faster phytoplankton growth in the Canary CS relative to the California CS, other mechanisms affecting the

BGD
8, 5617–5652, 2011

biomass but independent of the growth rate must contribute to the large NPP contrasts between the two systems.

According to Eq. (1), we can write the time-evolution of the phytoplankton biomass as:

$$\frac{\mathrm{d}P}{\mathrm{d}t} = \left[\mu_P(T,I,N_\mathrm{n},N_\mathrm{r}) - \Phi^{\mathrm{graz}}(P,Z) - \Phi^{\mathrm{mort}} - \Phi^{\mathrm{coag}}(P,D_\mathrm{S})\right]\cdot P + \nabla_{\mathrm{trans}}(P) \quad (6)$$

Where the term between square brackets on the right-hand side represents the net growth, i.e., growth minus the biological sink terms, and $\nabla_{\mathrm{trans}}(P)$ being the physical transport operator. Because of their very small magnitude, the phytoplankton mortality and the coagulation terms contribute very little to the net growth which is, therefore, essentially set by the balance between phytoplankton growth and the grazing by zooplankton (Fig. 8). Moreover, by examining the relationship between the grazing term $\Phi^{\mathrm{graz}}(P,Z)$ and the growth rate $\mu_P(T,I,N_\mathrm{n},N_\mathrm{r})$, we found very tight correlation between the two terms in both systems ($R^2 > 0.95$) (Fig. 9a). This results in the net growth being nearly proportional to the phytoplankton growth (Fig. 9b).

Therefore, if we consider an individual water particle and adopting a Lagrangian framework, Eq. (6) can be simplified to:

$$\frac{\mathrm{d}P}{\mathrm{d}t} \approx \alpha\cdot\mu_P(T,I,N_\mathrm{n},N_\mathrm{r})\cdot P \quad (7)$$

where α is a proportionality factor. This is a first order ordinary differential equation which can be solved if the Lagrangian time-evolution of the growth rate is known. In the idealized case where the growth rate remains constant within the narrow upwelling zone for particles reaching the surface, the solution of Eq. (7) is an exponential of the growth rate and the water residence time in the coastal zone.

Therefore, it appears that the previously shown partial decoupling between the growth rate on the one hand and the phytoplankton biomass and productivity on the other hand can result from contrasting residence times in the nearshore area between the two upwelling systems. Fast growth of phytoplankton may lead, indeed, to relatively low production levels if not associated with enough long water residence times.

BGD
8, 5617–5652, 2011

Conversely, long water residence times in the nearshore area can result in relatively large buildup of biomass, thereby leading to large production even at moderate growth levels.

Next, we investigate how water residence times in the nearshore vary between and within these systems, and we explore the potential mechanisms responsible for these variations as well as the impact this has on the recycling and export of nutrients and organic matter.

4 Discussion

4.1 Water residence times in the California and the Canary systems

The buildup of biomass in the upwelling zone is a function of the water renewal rate, i.e. the inverse of the residence time, in the nearshore area. To evaluate the water mass residence times in the upwelling zone, a large number of virtual particles were launched in this region and their Lagrangian trajectories computed using ARIANE (Blanke and Raynaud, 1997), a Lagrangian diagnostic tool fully documented at http://stockage.univ-brest.fr/~grima/Ariane/doc.html. For a good sampling of newly upwelled waters, we seeded each grid point in the near-surface (upper 10 m) and within the 50 km wide coastal strip. Repeating this particle release experiment each 5 days from April through August led to more than 100 000 particle trajectories in each of the two upwelling systems. Based on these large populations of individual trajectories, we statistically estimated the residence times of newly upwelled water masses in the 100 km wide nearshore area. Figure 10 shows the estimated water mass residence times in the Canary CS and California CS. The newly upwelled water stays on average around 33 days in the nearshore area of the Canary CS, which is twice as longer as in the the California CS. This enhances the buildup of biomass in the Canary CS coastal zone, leading to a substantially larger productivity in comparison with the California CS. Conversely, the substantially shorter water residence times in the nearshore

BGD
8, 5617–5652, 2011

region of the California CS result in an overall lower average biomass, thereby contributing to lowering the productivity in this system. Next, we explore the mechanisms potentially responsible for the identified contrasts in water residence times between the two systems.

4.2 The role of eddies and the shelf topography

Longer water residence time in the Canary CS relative to the California CS has no single explanation. The shelf topography and the level of eddy activity probably both contribute (Marchesiello and Estrade, 2009; Gruber et al., 2011). In order to test these hypotheses, we made three additional simulations. First, to evaluate the control of mesoscale eddies on the nearshore water residence times, we compare our control California CS simulation to analogous simulation where the momentum equation was linearized in such a way to suppress the eddy-driven transport in the model (Fig. 10a). The water residence times in the nearshore area are on average 70 % longer in the non-eddying simulation in comparison with the control eddying simulation. This confirms the important role exerted by mesoscale eddies in enhancing the offshore export and limiting the local buildup of biomass, in-line with the findings of Gruber et al. (2011). Second, to test the role of wide continental shelves in increasing water residence times, we made two additional Canary CS simulations at slightly coarser horizontal resolution of 15 km: (i) a first simulation where all the settings are kept identical to the control 5 km simulation, and (ii) a sensitivity experiment simulation where the initially wide continental shelf was narrowed on average by 30 % by altering the nearshore bottom topography. The 15 km Canary CS simulation with unaltered topography shows on average a 15 % longer residence times in comparison to the 5 km simulation (Fig. 10b). This is consistent with our previous finding that lower eddy activity leads to longer residence times in the nearshore area of EBUS. In the narrowed continental shelf simulation, the water residence times get, however, substantially reduced by 23 % on average (Fig. 10b). This confirms, therefore, the role of wide continental shelves in enhancing the local recycling and limiting the offshore export of nutrients and biomass. Our result

BGD
8, 5617–5652, 2011

is consistent with previous findings by Austin and Lentz (2002) and Marchesiello and Estrade (2009) based on idealized models. Next, we investigate the consequences of these differences for the recycling and export of nutrients and organic matter in the two upwelling systems.

4.3 Recycling and export of nutrients and organic matter in the California and the Canary systems

Inefficient use of nutrients combined with a relatively high offshore export of biomass leads in the California CS to less recycling of nutrients in the nearshore area, and thus a higher f-ratio, i.e., the ratio of new production to net primary production, in comparison with the Canary CS. Figure 11 shows the regenerated production as a function of the new production averaged over the first 100 km from the coast in both systems. While the new production is only 15 % lower in the California CS in comparison with the Canary CS, the regenerated production is almost twice smaller in the former. This leads to average f-ratios of 0.44 and 0.33 in the nearshore of the California CS and Canary CS, respectively.

Equating the new and export production over large spatial and temporal scales has been accepted in the community over decades (Eppley and Peterson, 1979). Yet, more recent studies revealed that these two fluxes can become spatially decoupled in coastal upwelling systems because of substantial offshore transport of newly produced organic matter (Berger et al., 1989; Plattner et al., 2005). Given the substantial differences found between the California and the Canary systems in terms of water residence times in the nearshore, we explore here how the relationship of export production to new production varies between these two systems.

In the California CS, the export production is generally smaller than the new production over the first 300 km from the coast, and larger further offshore with regression slopes of 0.53(±0.22) and 1.32(±0.23) in the two offshore regions, respectively (Fig 12). This is consistent with the results of Plattner et al. (2005) who found a substantial decoupling between new and export production in the California CS with

BGD
8, 5617–5652, 2011

a decoupling length-scale of 300 km. In contrast, in the Canary CS the values of the export and new production are, on average, very close to each other over the first 300 km from the coast (regression slope of 1.04(±0.38)), whereas in the 300–500 km offshore area the relationship between the new production and the export production is very similar to that in the California CS with nearly identical regression slopes (regression slope of 1.33(±0.25)). We interpret the relatively small differences between export and new production in the Canary CS as an indicator of a much stronger coupling between new and export production in this system in comparison to the California CS.

5 Summary and conclusions

We investigated the major drivers of the biological productivity in EBUS using a comparative modeling study of two of the four major EBUS, namely the California CS and the Canary CS. Our aim has been to identify and compare the productivity limitations in these two systems, and to explore the mechanisms that control the sensitivity of biological production to upwelling-favorable wind forcing.

Comparable eddy-resolving simulations of the California CS and the Canary CS show that although nutrient concentrations are on average about 20 % larger in the first, the primary production is 50 % larger in the second. By analyzing the phytoplankton growth in nutrient-replete conditions, we found that the more efficient use of nutrients in the Canary CS is essentially due to a more favorable light and temperature conditions, resulting in about 12 % faster growth in the Canary CS in comparison with the California CS. Yet, comparable growth rates in the Canary CS and the California CS are associated with substantially larger productivities in the former. This is due to large contrasts in the water renewal rates in the nearshore between the two systems.

We found that the newly upwelled water stays on average twice longer in the nearshore area of the Canary CS relative to the California CS. This enhances the buildup of biomass in the coastal zone of the Canary CS and leads to higher productivity, larger local recycling of nutrients and much stronger coupling between the new and

BGD
8, 5617–5652, 2011

export production. Two mechanisms were proposed and tested to explain the longer water residence time in the Canary CS relative to the California CS. First, the wider continental shelf in the Canary CS was shown to substantially increase the water residence time in the nearshore region in line with previous idealized model based studies. Second, the lower level of eddy activity in the Canary CS relative to the California CS was also tested as an additional factor explaining the relatively long water residence times in the coastal region of this system.

Overall, our results show that factors affecting timescales of biological growth such as the light and temperature and those related to the dynamics of the cross-shore circulation in coastal upwelling systems such as the shelf topography and the level of eddy activity exert a strong control on nutrient use efficiency, and thus, on the sensitivity of biological productivity to the intensity of upwelling. Therefore, this study suggests that the biological response to climate change induced perturbations such as upwelling favorable wind intensification (e.g., Bakun, 1990) or increased stratification (e.g., Rykaczewski and Dunne, 2010) might lead to contrasting biological responses in the California CS and the Canary CS, with major implications for the biogeochemical cycles and fisheries in these two ecosystems.

Acknowledgements. Support for this research has come from the Swiss Federal Institute of Technology Zurich (ETH Zurich). Computations were performed at the central computing cluster of ETH Zurich, Brutus. We thank the various providers of the satellite data, in particular the SeaWiFS Project (Code 970.2) sponsored by NASAs Mission to Planet Earth program, as well as the AVHRR data products sponsored by the NOAA/NASA Polar Pathfinder program.

References

Allen, J.: Upwelling and coastal jets in a continuously stratified ocean, J. Phys. Oceanogr., 3, 245–257, 1973. 5619

Aristegui, J., Barton, E. D., Tett, P., Montero, M. F., García-Muñoz, M., Basterretxea, G., Cussatlegras, A., Ojeda, A., and de Armas, D.: Variability in plankton community structure,

BGD

8, 5617–5652, 2011

metabolism, and vertical carbon fluxes along an upwelling filament (Cape Juby, NW Africa), Progress Oceanogr., 62, 95–113, doi:10.1016/j.pocean.2004.07.004, 2004. 5619
Aristegui, J., Barton, E. D., Alvarez-Salgado, X. A., Santos, M., Figuerias, F. G., Kifani, S., Hernandez-Leon, S., Mason, E., Machu, E., and Demarcq, H.: Sub-regional ecosystem variability in the Canary Current upwelling, Progress Oceanogr., 83, 33–48, doi:10.1016/j.pocean.2009.07.031, 2009. 5623
Austin, J. A. and Lentz, S. J.: The inner shelf response to wind-driven upwelling and downwelling, J. Phys. Oceanogr., 32, 2171–2193, 2002. 5633
Bakun, A.: Global climate change and intensification of coastal ocean upwelling, Science, 247, 198–201, doi:10.1126/science.247.4939.198, 1990. 5619, 5620, 5635
Barnier, B., Siefried, L., and Marchesiello, P.: Thermal forcing for a global ocean circulation model using a three-year climatology of ECMWF analyses, J. Mar. Syst., 6, 363–380, 1995. 5624
Beckmann, A. and Haidvogel, D. B.: Numerical simulation of flow around a tall isolated seamount. Part I: Problem formulation and model accuracy, J. Phys. Oceanogr., 23, 1736–1753, 1993. 5621
Berger, W. H., Smetacek, V. S., and Wefer, G.: Ocean productivity and paleoproductivity – an overview, in: Productivity of the Ocean: Present and Past, edited by: Berger, W. H., Smetacek, V. S., and Wefer, G., John Wiley, Hoboken, NJ, 1–35, 1989. 5633
Blanke, B. and Raynaud, S.: Kinematics of the Pacific Equatorial Undercurrent: an Eulerian and Lagrangian approach from GCM results, J. Phys. Oceanogr., 27, 1038–1053, 1997. 5631
Bograd, S. J., Castro, C. G., Di Lorenzo, E., Palacios, D. M., Bailey, H., Gilly, W., and Chavez, F. P.: Oxygen declines and the shoaling of the hypoxic boundary in the California Current, Geophys. Res. Lett., 35, L12607, doi:10.1016/S0967-0645(01)00094-7, 2008.
Brink, K.: The near-surface dynamics of coastal upwelling, Progress Oceanogr., 12, 223–257, doi:10.1016/0079-6611(83)90009-5, 1983. 5619
Carr, M.: Estimation of potential productivity in Eastern Boundary Currents using remote sensing, Deep-Sea Res. Pt. II, 49, 59–80, doi:10.1016/S0967-0645(01)00094-7, 2001. 5619, 5620
Carr, M. and Kearns, E. J.: Production regimes in four Eastern Boundary Current systems, Deep-Sea Res. Pt. II, 50, 3199–3221, doi:10.1016/j.dsr2.2003.07.015, 2003. 5618, 5619, 5620
Chan, F., Barth, J. A., Lubchenco, J., Kirincich, A., Weeks, H., Peterson, W. T., and

BGD
8, 5617–5652, 2011

Menge, B. A.: Emergence of anoxia in the California current large marine ecosystem, Science, 319(5865), 920, doi:10.1126/science.1149016, 2008.
Chassignet, E. P. and Verron, J.: Ocean Weather Forecasting: an Integrated View of Oceanography, Springer, Dordrecht, The Netherlands, 2006. 5623
Chavez, F. P. and Toggweiler, J. R.: Physical estimates of global new production: The upwelling contribution, in: Upwelling in the Ocean: Modern Processes and Ancient Records, edited by: Summerhayes, C. P., Emeis, K.-C., Angel, M. V., Smith, R. L., and Zeitzschel, B., 313–320, ISBN:978-0471960416, John Wiley, New York, 1995. 5619
Chavez, F. P. and Messié, M.: A comparison of eastern boundary upwelling ecosystems, Progress Oceanogr., 83, 80–96, doi:10.1016/j.pocean.2009.07.032, 2009.
da Silva, A. M., Young, C. C., Levitus, S.: Atlas of surface marine data 1994. Volume 1: algorithms and procedures. Technical Report NOAA Atlas NESDIS 6, National Oceanic and Atmospheric Administration, Washington, DC, 1994. 5624
de Boyer Montégut, C., Madec, G., Fischer, A. S., Lazar, A., and Iudicone, D.: Mixed layer depth over the global ocean: an examination of profile data and a profile-based climatology, J. Geophys. Res., 109, C12003, doi:10.1029/2004JC002378, 2004. 5626, 5643
Demarcq, H.: Trends in primary production, sea surface temperature and wind in upwelling systems (1998–2007), Progress Oceanogr., 83, 376–385, doi:10.1016/j.pocean.2009.07.022, 2009. 5620
Falkowski, P. G. and Raven, J.: Aquatic Photosynthesis, Blackwell, Oxford, 375 pp., 1997. 5629
FAO: The State of World Fisheries and Aquaculture 2008, Food & Agriculture Org, Pap/Cdr edn., 2009. 5619
Eppley, R. W.: Temperature and phytoplankton growth in the sea, Fish. B-NOAA, 70, 1063–1085, 1972. 5622
Eppley, R. W., and Peterson, B. J.: Particulate organic matter flux and planktonic new production in the deep ocean, Nature, 282, 677–680, 1979. 5633
Feely, R. A., Sabine, C. L., Hernandez-Ayon, J. M., Ianson, D., and Hales, B.: Evidence for upwelling of corrosive “acidified” water onto the continental shelf, Science, 320(5882), 1490–1492, 2008.
Gruber, N., Frenzel, H., Doney, S. C., Marchesiello, P., McWilliams, J. C., Moisan, J. R., Oram, J., Plattner, G.-K., and Stolzenbach, K. D.: Eddy-resolving simulation of plankton ecosystem dynamics in the California Current System, Deep-Sea Res. Pt. I, 53, 1483–1516, doi:10.1016/j.dsr.2006.06.005. 2006 5621, 5623, 5624, 5625, 5627

BGD
8, 5617–5652, 2011

Gruber, N., Lachkar, Z., Frenzel, H., Marchesiello, P., Munnich, M., McWilliams, J. C., Nagai, T., and Plattner, G.: Mesoscale eddy-induced reduction of biological production in coastal upwelling systems, Nature Geosci., submitted, 2011. 5620, 5632

Hyde, K., O'Reilly, J., and Oviatt, C.: Validation of SeaWiFS chlorophyll-*a* in Massachusetts Bay, Cont. Shelf Res., 27, 1677–1691, 2007. 5625

Kahru, M., Kudela, R., Manzano-Sarabia, M., and Mitchell, B. G.: Trends in primary production in the California Current detected with satellite data, J. Geophys. Res., 114, C02004, 2009.

Lachkar, Z. Gruber, N., and Plattner, G.-K.: A comparative study of biological productivity in eastern boundary upwelling systems using an artifical neural network, Biogeosciences, in preparation, 2011. 5619, 5620

Large, W. G., McWilliams, J. C., and Doney, S. C.: Oceanic vertical mixing: A review and a model with a nonlocal boundary layer parameterization, Rev. Geophys. Res., 32, 363–403, 1994. 5621

Marchesiello, P. and Estrade, P.: Eddy activity and mixing in upwelling systems: a comparative study of Northwest Africa and California regions, Int. J. Earth Sci., 98, 299–308, doi:10.1007/s00531-007-0235-6, 2009. 5620, 5632, 5633

Marchesiello, P., McWilliams, J. C., and Shchepetkin, A. F.: Open boundary conditions for long-term integration of regional oceanic models, Ocean Model., 3, 1–20, 2001. 5621

Marchesiello, P., McWilliams, J. C., and Shchepetkin, A. F.: Equilibrium structure and dynamics of the California Current system, J. Phys. Oceanogr., 33, 753–783, 2003. 5621

McGregor, H. V., Dima, M., Fischer, H. W., and Mulitza, S.: Rapid 20th-century increase in coastal upwelling off Northwest Africa, Science, 315, 637–639, doi:10.1126/science.1134839, 2007. 5620

Mendelssohn, R. and Schwing, F. B.: Common and uncommon trends in SST and wind stress in the California and Peru-Chile current systems, Progress Oceanogr., 53(2–4), 141–162, ISSN:0079–6611, doi:10.1016/S0079-6611(02)00028-9, 2002. 5620

Muller-Karger, F. E., Varela, R., Thunell, R., Luerssen, R., Hu, C., and Walsh, J. J.: The importance of continental margins in the global carbon cycle, Geophys. Res. Lett., 32, L01602, 2005. 5619

Pauly, D. and Christensen, V.: Primary production required to sustain global fisheries, Nature, 374, 255–257, doi:10.1038/374255a0, 1995. 5619

Plattner, G.-K., Gruber, N., Frenzel, H., and McWilliams, J. C.: Decoupling marine export production from new production, Geophys. Res. Lett., 32, L11612, 2005.

BGD

8, 5617–5652, 2011

Risien, C. M., and Chelton, D. B.: A global climatology of surface wind and wind stress fields from eight years of QuikSCAT scatterometer data, J. Phys. Oceanogr., 38, 2379–2413, 2008. 5633

Rossi, V., López, C., Sudre, J., Hernández-García, E., and Garçon, V.: Comparative study of mixing and biological activity of the Benguela and Canary upwelling systems, Geophys. Res. Lett., 35, L11602, doi:10.1029/2008GL033610, 2008. 5624

Rykaczewski, R. R. and Dunne, J. P.: Enhanced nutrient supply to the California Current Ecosystem with global warming and increased stratification in an Earth system model, Geophys. Res. Lett., 37, L21606, doi:10.1029/2010GL045019, 2010. 5620

Schollaert, S. E., Yoder, J. A., O'Reilly, J. E., and Westphal, D. L.: Influence of dust and sulfate aerosols on ocean color spectra and chlorophyll-*a* concentrations derived from SeaWiFS off the US east coast, J. Geophys. Res., 108(C6, 3191), 1–13, 2003. 5635

Schwing, F. B. and Mendelssohn, R.: Increased coastal upwelling in the California Current System, J. Geophys. Res., 102(C2), 3421–3438, doi:10.1029/96JC03591, 1997. 5625

Shannon, L., Crawford, R., Pollock, D., Hutchings, L., Boyd, A., Taunton-Clark, J., Badenhorst, A., Melville-Smith, R., Augustyn, C., Cochrane, K., Hampton, I., Nelson, G., Japp, D., and Tarr, R.: The 1980s a decade of change in the Benguela ecosystem, S. Afr. J. Marine Sci., 12, 271–296, 1992.

Shchepetkin, A. F. and McWilliams, J. C.: Quasi-monotone advection schemes based on explicit locally adaptive dissipation, Monthly Weather Rev., 126, 1541–1580, 1998. 5620

Shchepetkin, A. F. and McWilliams, J. C.: The regional oceanic modeling system (ROMS): A split-explicit, free-surface, topography-following-coordinate oceanic model, Ocean Modell. IX, pp. 347–404, Hooke Inst. Oxford Univ., Oxford, UK, 2005. 5621

Smith, W. H. F. and Sandwell, D. T.: Global seafloor topography from satellite altimetry and ship depth soundings, Science, 277, 1957–1962, 1997. 5621

Taylor, K. E.: Summarizing multiple aspects of model performance in a single diagram, J. Geophys. Res., 106, 7183–7192, 2001. 5621

Thomas, A. C., Carr, M.-E., and Strub, P. T.: Chlorophyll variability in Eastern Boundary Currents, Geophys. Res. Lett., 28(18), 3421–3424, 2001. 5625, 5643

Wroblewski, J. S.: A model of phytoplankton plume formation during variable Oregon upwelling, J. Marine Res., 35, 357–394, 1977. 5619, 5620

5623

BGD

8, 5617–5652, 2011

Table 1. Productivity and its drivers averaged over the 300 km wide nearshore area for the California CS and the Canary CS. T_{resid} refers to the water residence time in the 100 km wide nearshore area. The last three columns show normalized nutrient-replete growth rates μ_P^{max} to constant PAR = 20 W m^{-2}, θ = 25 mg C (mg chl-a)$^{-1}$ and T = 20 °C, respectively.

	NPP	TIN	T_{resid}	μ_P	μ_P^{max} (I = const)	μ_P^{max} (θ = const)	μ_P^{max} (T = const)	μ_P^{max}
Unit	mol C m^{-2} yr^{-1}	mol C m^{-2}	day	day^{-1}	day^{-1}	day^{-1}	day^{-1}	day^{-1}
California CS	11.8	2.63	17.36	0.32	0.46	0.45	0.52	0.5
Canary CS	18.15	2.17	33.18	0.36	0.64	0.42	0.83	0.63
Relative diff.	+54 %	−18 %	+91 %	+12 %	+40 %	−7 %	+60 %	+26 %

BGD
8, 5617–5652, 2011

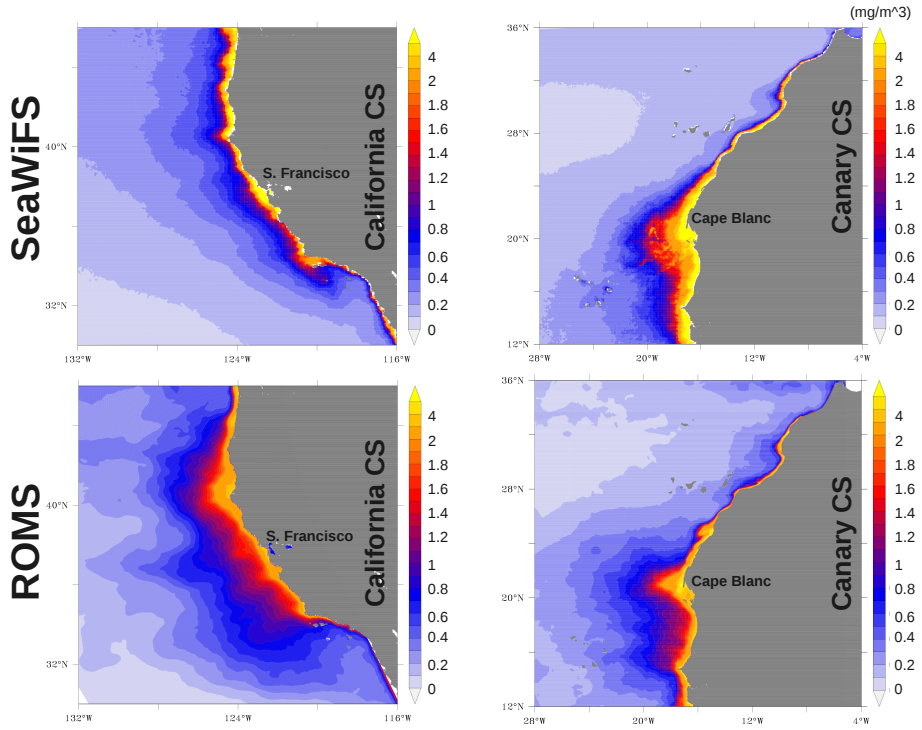

Fig. 1. Annual average of surface chlorophyll-*a* concentrations (mg m^{-3}) from SeaWiFS (top) and ROMS model (bottom) in the California CS (left) and the Canary CS (right). The SeaWiFS climatology is computed over the period from 1997 to 2007.

BGD
8, 5617–5652, 2011

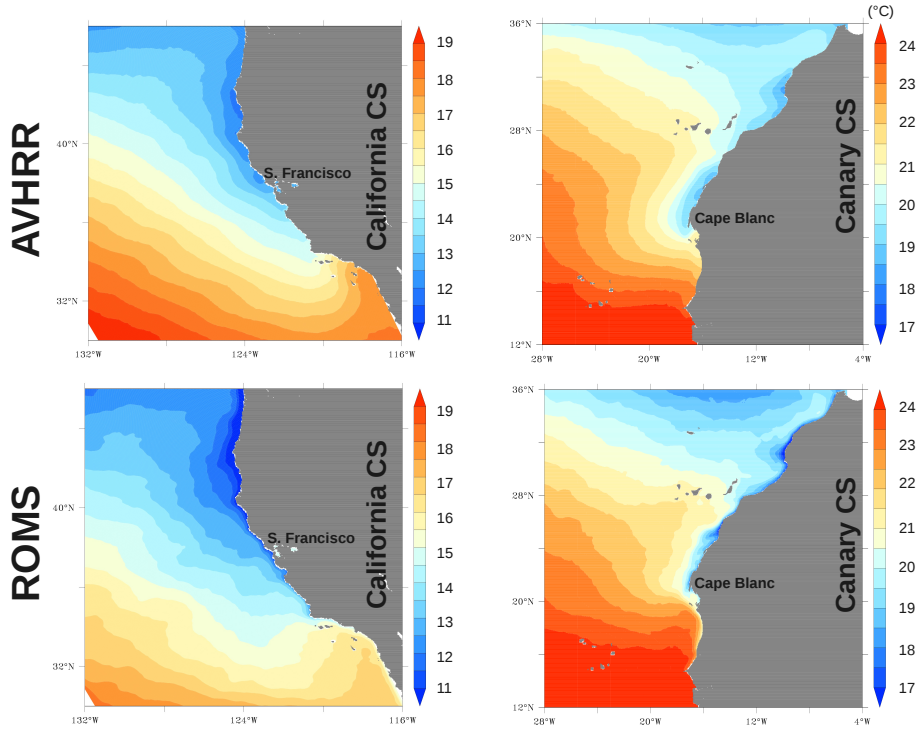

Fig. 2. Sea surface temperature (SST) annual average (°C) from AVHRR (top) and ROMS model (bottom) in the California CS (left) and the Canary CS (right). The AVHRR observational climatology is computed over the period from 1997 to 2005.

BGD
8, 5617–5652, 2011

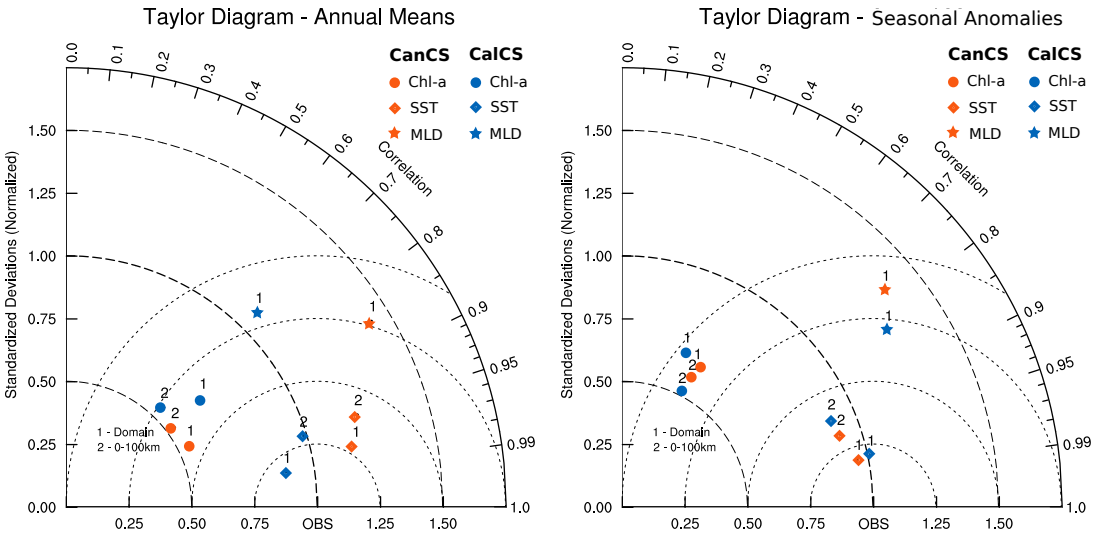

Fig. 3. Taylor (2001) diagrams of modeled annual-mean (left) and seasonal anomalies (right) of surface chlorophyll (circles), sea surface temperature (diamonds) and mixed layer depth (stars) in the California CS (blue) and the Canary CS (orange). The reference point of the Taylor diagram corresponds to SeaWiFS observations for chlorophyll, AVHRR data for temperature and the monthly climatology of de Boyer Montégut et al. (2004) for the mixed layer depth. The statistics were computed separately for the entire domain (data points labeled "1") and the 100 km wide nearshore region (data points labeled "2").

BGD
8, 5617–5652, 2011

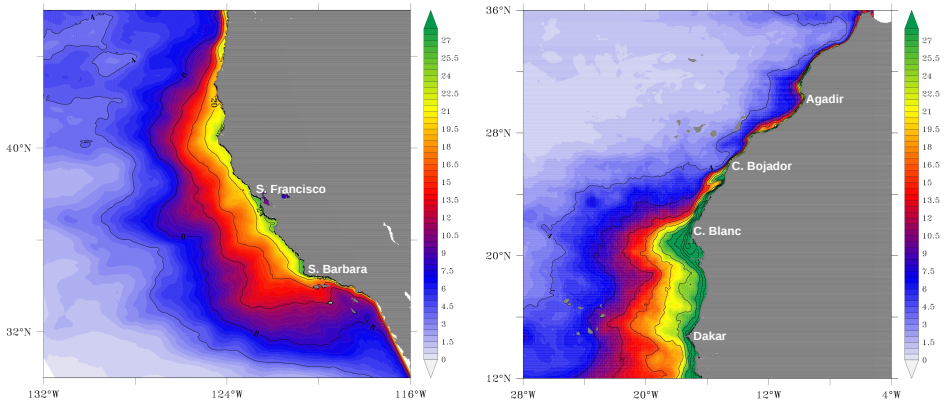

Fig. 4. Simulated annual mean, vertically integrated NPP (mol C m^{-2} yr^{-1}) in the California CS (left) and Canary CS (right).

BGD
8, 5617–5652, 2011

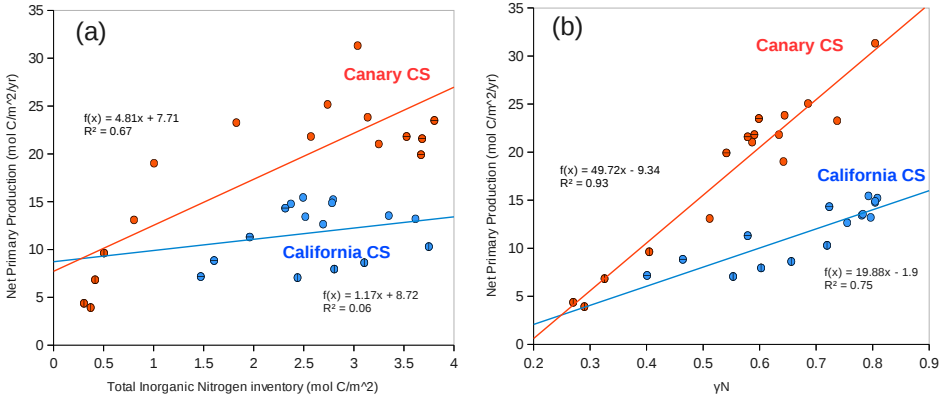

Fig. 5. **(a)** The relationship between NPP and the inventory of TIN in the euphotic zone in the California CS (blue) and Canary CS (orange). **(b)** NPP as a function of the nutrient limitation factor $\gamma(N_n, N_r)$ averaged over the upper 40 m in the California CS (blue) and Canary CS (orange). Data were averaged over the 300 km wide nearshore area and over 1° bins in meridional direction. Circles with horizontal lines correspond to the southernmost part of each system, i.e., from 30° N to 34° N for the California CS and from 12° N to 16° N for the Canary CS, and circles with vertical lines indicate their northernmost parts, i.e., from 42° N to 46° N for the California CS and from 24° N to 28° N for the Canary CS.

BGD
8, 5617–5652, 2011

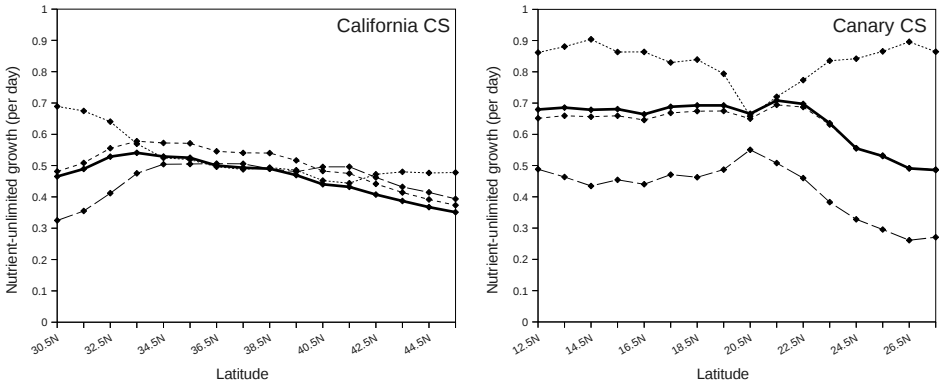

Fig. 6. Meridional distribution of the temperature-dependent, light-limited growth rate under nutrient replete conditions $\mu_P^{\max}(T,I)$ in the California CS (left) and the Canary CS (right). Data is horizontally averaged over the 300 km wide nearshore area and vertically over the upper 40 m. Shown are the simulated $\mu_P^{\max}(T,I)$ (solid) and normalized $\mu_P^{\max}(T,I)$ to to constant PAR = 20 W m^{-2} (long dashed), temperature $T = 20\,^{\circ}$C (fine dashed) and chlorophyll-to-carbon ratio $\theta = 25$ mg C (mg Chl-a)$^{-1}$ (dotted).

BGD
8, 5617–5652, 2011

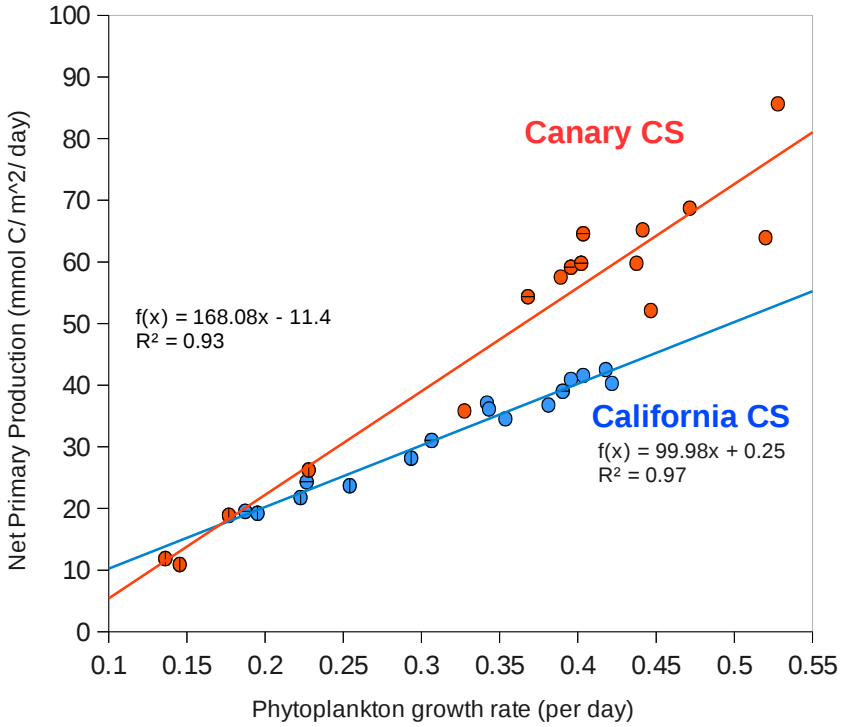

Fig. 7. The relationship between NPP and the phytoplankton growth rate in the California CS (blue) and Canary CS (orange). Data were averaged over the 300 km wide nearshore area and over 1° bins in meridional direction. Circles with horizontal lines correspond to the southernmost part of each system, i.e., from 30° N to 34° N for the California CS and from 12° N to 16° N for the Canary CS, and circles with vertical lines indicate their northernmost parts, i.e., from 42° N to 46° N for the California CS and from 24° N to 28° N for the Canary CS.

BGD
8, 5617–5652, 2011

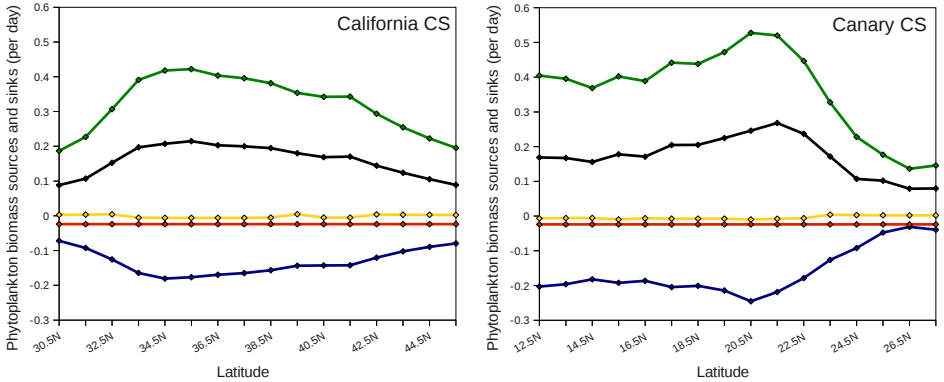

Fig. 8. Meridional distribution of the net growth of phytoplankton (black) and its four components: the growth (green), the grazing (blue), the mortality (red) and the coagulation (yellow) daily rates in the California CS (left) and the Canary CS (right). Data is horizontally averaged over the 300 km wide nearshore area and vertically over the upper 40 m.

BGD
8, 5617–5652, 2011

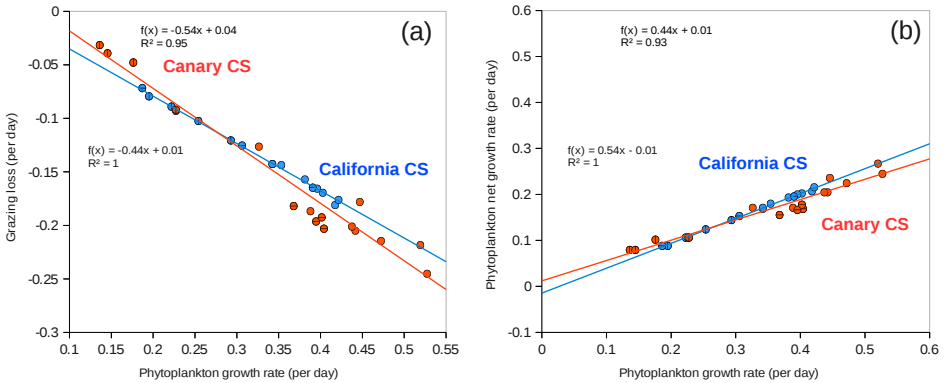

Fig. 9. **(a)** The grazing rate as a function of the growth rate in the California CS (blue) and Canary CS (orange). **(b)** The net growth rate as a function of the growth rate in the California CS (blue) and Canary CS (orange). Data were averaged over the 300 km wide nearshore area and over 1° bins in meridional direction. Circles with horizontal lines correspond to the southernmost part of each system, i.e., from 30° N to 34° N for the California CS and from 12° N to 16° N for the Canary CS, and circles with vertical lines indicate their northernmost parts, i.e., from 42° N to 46° N for the California CS and from 24° N to 28° N for the Canary CS.

BGD
8, 5617–5652, 2011

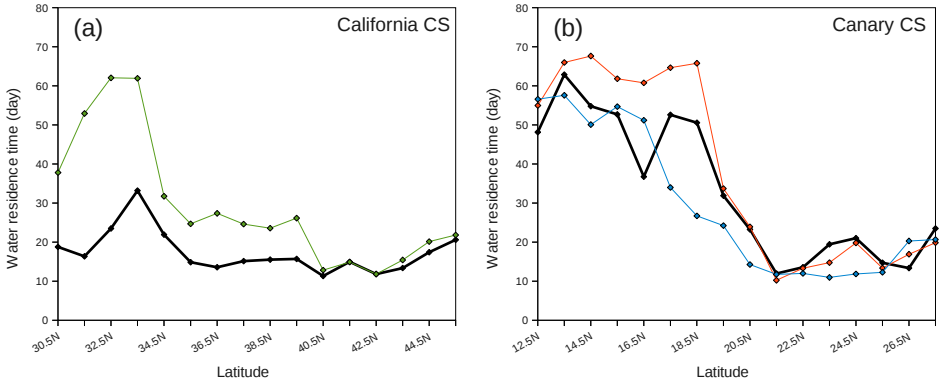

Fig. 10. (a) Meridional distribution of the water residence times in the 100 km wide nearshore area in the California CS as simulated in the control simulation (black) and the non-eddy simulation (green). **(b)** Meridional distribution of the water residence times in the 100 km wide nearshore area in the Canary CS as simulated in the control 5 km simulation (black), the 15 km simulation with unaltered topography (orange) and the 15 km narrowed-shelf simulation (blue).

BGD
8, 5617–5652, 2011

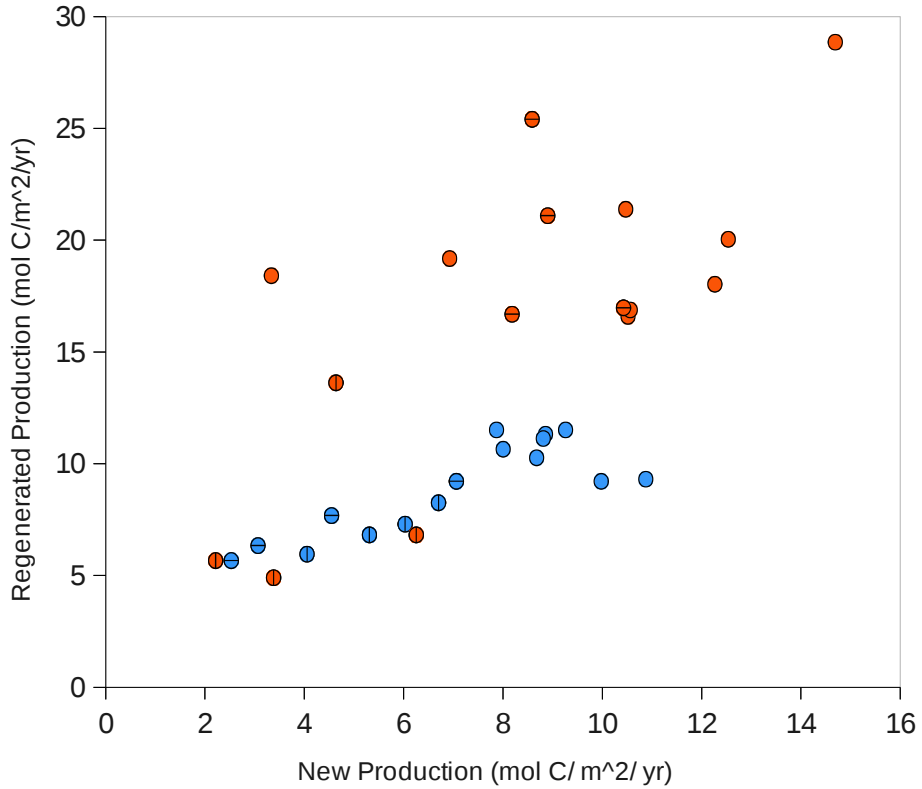

Fig. 11. The relationship between the regenerated production and the new production in the California CS (blue) and Canary CS (orange). Data were averaged over the 100 km wide nearshore area and over 1° bins in meridional direction. Circles with horizontal lines correspond to the southernmost part of each system, i.e., from 30° N to 34° N for the California CS and from 12° N to 16° N for the Canary CS, and circles with vertical lines indicate their northernmost parts, i.e., from 42° N to 46° N for the California CS and from 24° N to 28° N for the Canary CS.

BGD
8, 5617–5652, 2011

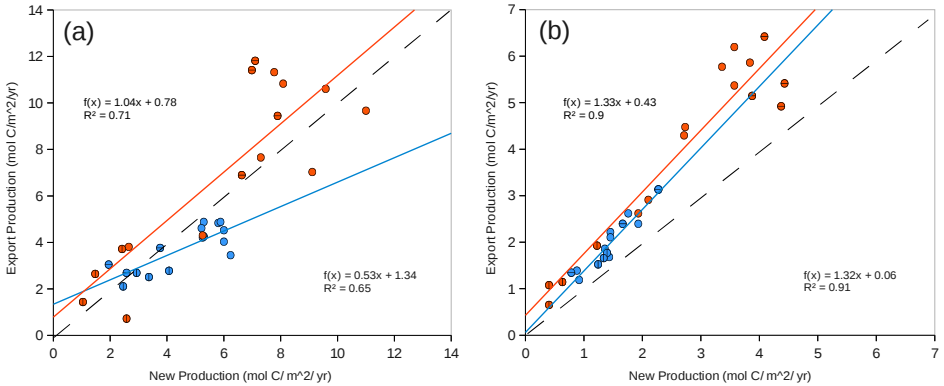

Fig. 12. Export production as a function of new production in the California CS (blue) and Canary CS (orange) averaged over the 300 km wide nearshore area (left) and between 300 km and 500 km offshore (right). Data were averaged over 1° bins in meridional direction. Circles with horizontal lines correspond to the southernmost part of each system, i.e., from 30° N to 34° N for the California CS and from 12° N to 16° N for the Canary CS, and circles with vertical lines indicate their northernmost parts, i.e., from 42° N to 46° N for the California CS and from 24° N to 28° N for the Canary CS. The diagonal dashed grey line indicate the identity line.

BGD
8, 5617–5652, 2011